Dilated cardiomyopathy myosin mutants have reduced force-generating capacity

Received for publication, January 30, 2018, and in revised form, April 14, 2018 Published, Papers in Press, April 17, 2018, DOI 10.1074/jbc.RA118.001938

Zoltan Ujfalusi[‡§1], Carlos D. Vera[¶1], Srbolujub M. Mijailovich[‖], Marina Svicevic[**], Elizabeth Choe Yu[‡‡], Masataka Kawana[§§], Kathleen M. Ruppel[§§], James A. Spudich[§§2,3], Michael A. Geeves[‡4], and Leslie A. Leinwand[¶2,5]

From the [‡]School of Biosciences, University of Kent, Canterbury CT2 7NJ, United Kingdom, the [¶]BioFrontiers Institute and Department of Molecular, Cellular, and Developmental Biology, University of Colorado, Boulder, Colorado 80309, the [‖]Department of Biology, Illinois Institute of Technology, Chicago, Illinois 60616, the [**]Faculty of Science, University of Kragujevac, Kragujevac 34000, Serbia, the Departments of [‡‡]Pediatrics (Cardiology) and [§§]Biochemistry, Stanford University School of Medicine, Stanford, California 94305, and the [§]Department of Biophysics, University of Pécs, Medical School, Szigeti Street 12, H-7624 Pécs, Hungary

Edited by Velia M. Fowler

Dilated cardiomyopathy (DCM) and hypertrophic cardiomyopathy (HCM) can cause arrhythmias, heart failure, and cardiac death. Here, we functionally characterized the motor domains of five DCM-causing mutations in human β-cardiac myosin. Kinetic analyses of the individual events in the ATPase cycle revealed that each mutation alters different steps in this cycle. For example, different mutations gave enhanced or reduced rate constants of ATP binding, ATP hydrolysis, or ADP release or exhibited altered ATP, ADP, or actin affinity. Local effects dominated, no common pattern accounted for the similar mutant phenotype, and there was no distinct set of changes that distinguished DCM mutations from previously analyzed HCM myosin mutations. That said, using our data to model the complete ATPase contraction cycle revealed additional critical insights. Four of the DCM mutations lowered the duty ratio (the ATPase cycle portion when myosin strongly binds actin) because of reduced occupancy of the force-holding A·M·D complex in the steady state. Under load, the A·M·D state is predicted to increase owing to a reduced rate constant for ADP release, and this effect was blunted for all five DCM mutations. We observed the opposite effects for two HCM mutations, namely R403Q and R453C. Moreover, the analysis predicted more economical use of ATP by the DCM mutants than by WT and the HCM mutants. Our findings indicate that DCM mutants have a deficit in force generation and force-holding capacity due to the reduced occupancy of the force-holding state.

Dilated cardiomyopathy (DCM)[6] and hypertrophic cardiomyopathy (HCM) are significant causes of arrhythmias, heart failure, and sudden cardiac death (1). Whereas many cases are idiopathic, mutations in proteins of the cardiac sarcomere, including β-cardiac myosin, can cause both diseases. DCM is characterized by a dilated ventricular cavity with systolic dysfunction and is a very heterogeneous disease from an etiologic standpoint. HCM is characterized by preserved or enhanced systolic function and significant hypertrophy (2–4).

Whereas most mutations that cause HCM are in sarcomeric proteins, the genetics of familial DCM are much more diverse, with mutations in titin being the most common (5, 6). That said, more than 30% of HCM-causing mutations and 3– 4% of DCM-causing mutations are found in the β-myosin heavy-chain gene, *MYH7* (6, 7). DCM-causing mutations in the β-cardiac myosin gene are found in different domains of the motor and in the tail region, although penetrance of the tail region mutations is incomplete (8). We selected five DCM-causing mutations in the β-cardiac myosin motor domain for study (their locations in the motor domain are shown in Fig. 1). These include S532P and F764L (9). Affected individuals presented with early-onset ventricular dilatation without antecedent symptoms or signs of hypertrophy and often progressed to heart failure. A223T was identified in a 35-year-old male DCM patient (10). R237W, a possible disease-causing mutation, was identified in a patient with familial DCM (11). The fifth DCM mutation we chose to study is I201T, which can cause ventricular dilatation with or without systolic dysfunction (12).

In our previous studies, we completed detailed characterization of the biochemical and chemo-mechanical properties of human β-cardiac myosin motor domains carrying either R403Q or R453C HCM mutations (13–15). For R453C, whereas there was a decrease in ATPase activity and *in vitro* motility, there was a 50% increase in intrinsic force (13). Kinetic measurements of this mutant motor showed subtle perturbations. The exceptions were the rate constants for ATP binding (reduced by 35%) and the ATP hydrolysis step/recovery stroke (slowed 3-fold) (15). In contrast, the human R403Q mutant motor showed an overall loss of func-

J. A. S. is a founder of and owns stock in MyoKardia, Inc. L. A. L. is a founder of, owns stock in, and has a sponsored research agreement with MyoKardia, Inc. The content is solely the responsibility of the authors and does not necessarily represent the official views of the National Institutes of Health.

This article contains Tables S1–S7 and Figs. S1–S7.

[1] Both authors contributed equally to this work.
[2] Supported by National Institutes of Health Grant HL117138.
[3] Supported by National Institutes of Health Grant GM33289.
[4] Supported by British Heart Foundation Grant PG-175-30200. To whom correspondence may be addressed: School of Biosciences, University of Kent, Canterbury CT2 7NJ, United Kingdom. E-mail: m.a.geeves@kent.ac.uk.
[5] To whom correspondence may be addressed: Dept. of Molecular, Cellular, and Developmental Biology, University of Colorado, Boulder CO 80309. E-mail: leslie.leinwand@Colorado.edu.

[6] The abbreviations used are: DCM, dilated cardiomyopathy; HCM, hypertrophic cardiomyopathy; sS1, short subfragment-1; β-sS1, short subfragment-1 with a single IQ domain; ELC, essential light chain; pN, piconewton(s).

tion (14). We published a modeling analysis of the WT β-cardiac S1 and the HCM mutation, R453C (16), which demonstrated that such detailed kinetic information on the individual molecular events in the ATPase cycle can be used to model the complete mechanochemical cycle and predict some of the properties of the motor, such as maximum shortening velocity, and the load dependence of force-holding states. In principle, the same approach should allow us to define how missense mutations alter the mechanochemical cycle and may provide insights into how mutations can cause different cardiac phenotypes.

Whereas many cell and mouse models have been made for HCM cardiac myosin mutations (17–19), there are fewer studies on myosin mutations that cause DCM. Two mouse models have been described, S532P and F764L, and some of the biochemical properties of myosin purified from the hearts of these mice have been described (20, 21). Contractile function was reduced, and purified mutant myosin from mouse hearts showed decreased actin-activated ATPase and *in vitro* motility. It is important to note that both of these models were made placing mutations into the mouse α-cardiac myosin gene as opposed to the human β-cardiac myosin gene. This point stems from the observation that the R403Q mutation was shown to have very different effects in the context of α-cardiac myosin compared with β-cardiac myosin (14, 22).

Here, we report detailed biochemical characterization and mechanochemical cycle modeling of recombinant human β-cardiac myosin motor domains carrying five DCM mutations. The data are compared with our previous data on the human β WT and the motor domain carrying either of two well-known HCM mutations (14, 15). Because each of these mutations produces clinically related hypocontractile DCM phenotypes, we might expect to see similar alterations in the properties of the mutant myosin motor domain, and we predict that these will be distinct from those seen for mutations that cause HCM. Our data indicate that each mutation has its own distinct effects on individual steps of the mechanochemical cycle, and the pattern of changes shows no commonality between DCM-linked mutations or distinct differences between DCM and HCM mutations. However, when the complete cycle is modeled, distinct behaviors do emerge. DCM mutations have lower occupancy of the force-holding A·M·D state in the steady state than WT or the HCM mutations for four of five DCM mutations. This predicts a lower duty ratio for the DCM mutations and a stronger effect of load on the cycle. Our analysis also suggests that DCM mutations use less ATP than WT in generating high force or high velocities. In contrast, the two HCM mutations have a similar efficiency as WT for force generation, and they are less efficient for high-velocity contraction.

Results

Location of the five mutations in the structure of the motor domain

The five DCM mutations studied here were selected because they are located in quite distinct regions of the motor domain and are highly conserved across myosins, and yet all cause DCM (Fig. 1, *A* and *B*). Three of the mutations are in the upper 50-kDa domain close to regions that may influence nucleotide binding. Ile-201 (mutated to Thr) is at the end of a helix that links the P-loop (which binds the γ P_i of ATP) to the start of loop 1, a surface loop known in many myosins as a variable loop that can influence the affinity of ADP for myosin and actin·myosin. (For a review of structures, see Refs. 23–25.) Ala-223 (mutated to Thr) is a buried residue near the ATP-binding site, in a helix just after loop 1, and the helix has potential interactions with major structural elements in the upper 50-kDa domain, such as helix O (which links the actin-binding cardiomyopathy loop to the nucleotide pocket) and the central β-sheet (strand 7). Arg-237 (mutated to Trp) is just before switch 1, a highly conserved region responsible for binding to the γ-phosphate of ATP. Closing of switch 1 onto ATP results in opening of the large cleft through the upper 50-kDa domain. This cleft spans the actin-binding site, and opening the cleft destroys the ability of myosin to bind strongly to actin. The change from the charged arginine to hydrophobic tryptophan could cause disruption in the local structure and movement of switch 1. The identical mutation in human myosin 1C (R156W) is reported to be associated with bilateral sensorineural hearing loss (26). Ser-532 (mutated to Pro) is in a small helix in the lower 50-kDa domain just before the actin-binding loop 3. Finally, Phe-764 (mutated to Leu) is in the converter region, which moves with the lever arm as the motor goes through its power stroke and its reversal, the recovery stroke (which is coupled to the ATP hydrolysis step). Thus, each mutation has the potential to perturb local interactions that are important for the efficient operation of the motor. The long-term question we are interested in is how each of these mutations in distinct domains results in similar clinical phenotypes.

Transient kinetic data

Recombinant human short subfragment-1 with a single IQ domain (β-sS1) for both WT and DCM-causing mutations was co-expressed in C_2C_{12} cells with a His-tagged or a FLAG-tagged human ventricular essential light chain (ELC). After elution from the affinity column, the proteins were dialyzed into experimental buffer and analyzed via SDS-PAGE (see Fig. 2) as described under "Experimental procedures."

In our previous studies, we completed a detailed characterization of the events in the myosin and actin·myosin ATPase for human β-S1 and the S1 carrying either R403Q or R453C mutations associated with HCM (14, 15). We were able to measure the rate and equilibrium constants for most of the events shown in Figs. 3 and 4 and used these together with steady-state ATPase data to model the behavior of the WT and R453C mutation (16). Here, we have taken the same approach to understand the molecular impact of the five DCM mutations.

The experimental methods and analysis tools used for the transient kinetic experiments have been extensively described in our previous publications (15, 27–29). The type of data, the quality of the signals, the reliability of the fitting programs, and assignments of fitted constants have been described previously (14, 15). In the interest of brevity, we present a summary of the data here with details of the measurements can be found in Figs. S1–S6 in the supporting information. The data are summarized in Table 1. Each assay was completed a minimum of three times

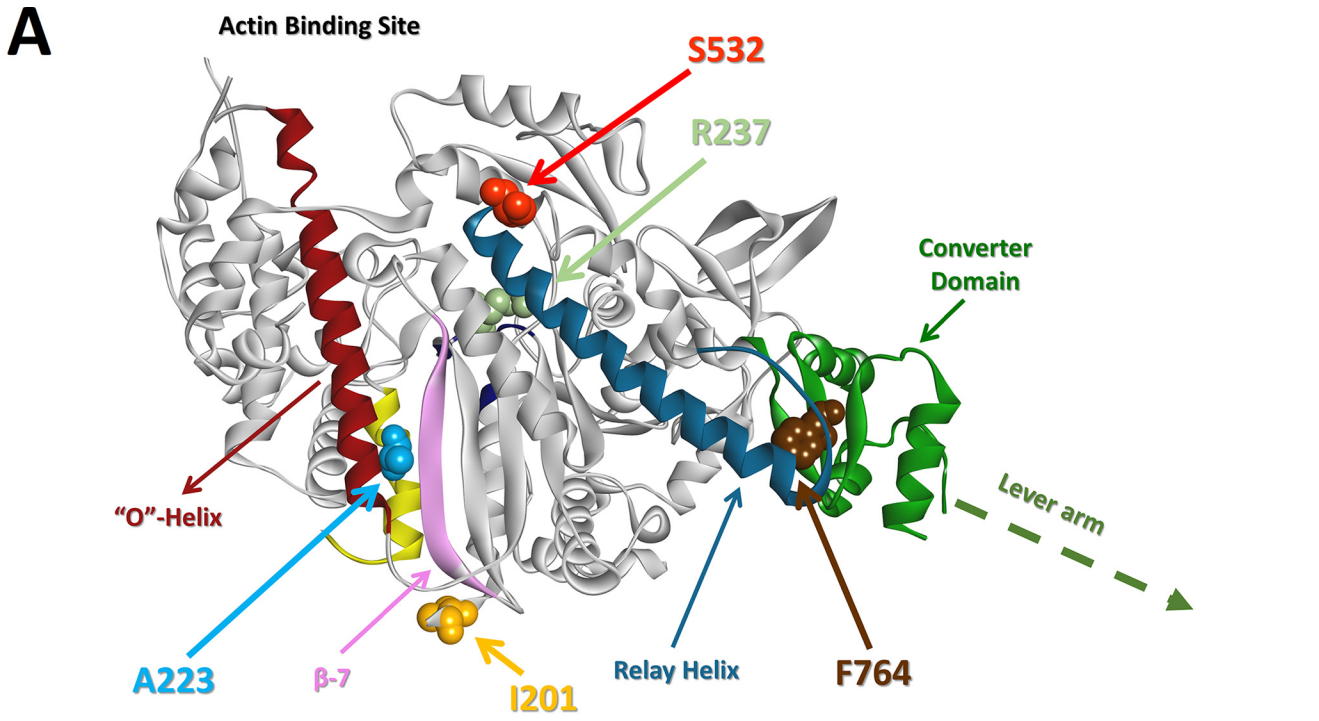

Figure 1. Structure and location of DCM mutations in the myosin motor domain. *A*, structural model of the motor domain of β-cardiac myosin (based on Protein Data Bank entry 4P7H). The main chain is shown as a *ribbon diagram* with the side chains of residues mutated in DCM patients and used in this study shown in *space-filling form*. Some key elements of the structure are *highlighted* in *color* to help orientate the reader. *B*, conservation of mutation sites in the myosin family. Example sequences are shown. The five residues are conserved for MYH7 in over 82 mammalian species (data not shown). Residues 237 and 764 are arginine and phenylalanine, respectively, across all myosins examined, emphasizing the functional importance of domains like the switch-1 and the converter domain and their highly conserved nature. Ser-532 is conserved in all mammalian myosin II and several other eukaryotes. Ala-223 is conserved in cardiac and some skeletal isoforms in most mammals. Ile-201 is conserved only in mammalian cardiac isoforms, as loop 1 is highly variable across species and isoforms.

with at least two different preparations purified from C_2C_{12} cells. In virtually every case, the data define each measured constant to better than 20%, giving high confidence in the measured values. The *background colors* in Table 1 indicate which values differ by >30% (*pale blue* or *red*) or >2-fold (*dark colors*) from the previously published WT values (14). In all cases, these values are statistically significantly different from the WT values (mostly at $p < 0.01$; see Table 1).

Implications of the data

These comprehensive data should be able to reveal any common patterns in the effects of these DCM mutations on the properties of the motor domain. However, the mutations are situated throughout the motor domain, and there may also be local effects of the mutation specific to the site of each mutation. In looking for such patterns, the expectation is that such similarities should be distinct from those of the previously described HCM mutations (14, 15). The data, as displayed in Table 1, do not make any such pattern easy to establish. We have therefore redisplayed the data in a series of histograms (Fig. 4).

Fig. 4*A* presents the data for the affinities of actin for the motor domain in the rigor complex (K_A) and in the presence of ADP (K_{DA}) and the apparent affinity of actin for myosin during the steady-state ATPase (K_m). Note that the salt concentrations used were lower in the ATPase assay (5 mM KCl) than in the K_A and K_{DA} measurements (25 mM KCl) and the temperature at 23 °C was 3 °C higher for the ATPase measurements than for the other kinetic assays.

The affinity of WT β-S1 for actin (K_A) was 10 ± 1.8 nM. In most cases, the affinity was weakened significantly by 25–125%, the exceptions being I201T, where it was similar to WT, and S532P, where it was apparently tighter, but such affinities (<10 nM) are difficult to measure with precision using our methods. In contrast, the affinity of β-S1 for actin in the presence of

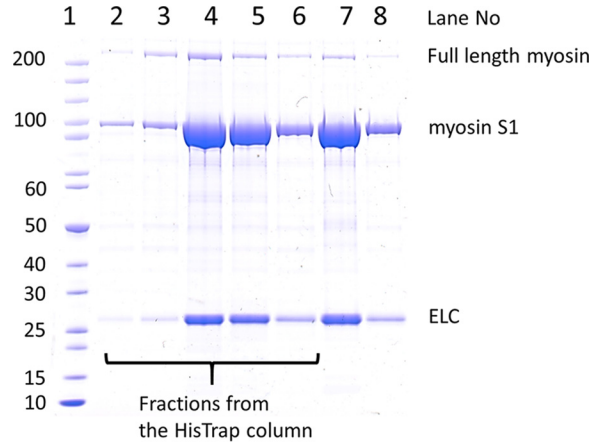

Figure 2. Image of a typical SDS-polyacrylamide gel of the human recombinant β-sS1 during purification. After the molecular weight markers (*lane 1*), the fractions from the His trap column are shown (*lanes 2–6*), followed by the pooled fractions, after dialysis, at two loading levels (*lanes 7* and *8*). The contaminant C_2C_{12} full-length myosin is estimated as ~1% by weight or 0.5% by molar ratio of sS1/full-length myosin.

saturating ADP (WT = 109 nM) was in four mutants significantly tighter (50–80%) but weaker for the A223T mutant (250%). The two HCM constructs were also weaker (25% for R403Q and 100% for R453C). Thus, no simple pattern emerged from these affinities that defined the DCM phenotype as distinct from the two HCM mutants.

Fig. 4*A* also includes the apparent affinities of ATP and ADP for sS1 ($1/K_1$, and K_6K_7 defined in Fig. 3). All DCM mutations showed a major weakening of the affinity of ATP for sS1, whereas the two HCM mutations showed only small changes, which may not be significant. In contrast, the ADP affinity for sS1 was generally tighter, but by a relatively small degree compared with the changes in ATP affinity. R237W is the exception and showed a 50% weaker ADP affinity. Because ATP and ADP do not bind to sS1 in the normal cross-bridge cycle, these events have little direct relevance to the DCM phenotypes, but no pattern emerges for the DCM *versus* HCM mutations.

In the case of ATP and ADP binding to actin·sS1 ($1/K_1'$ and $K_6'K_7'$, respectively), the ATP affinities had a modest tighter affinity (25–50%) except in the case of R237W (2-fold weaker). ADP affinities were weaker by 20–30% except in the case of R237W (4-fold weaker) and the HCM mutation R453C (almost 2-fold weaker). Again, there was no obvious pattern of behavior for the DCM *versus* HCM mutations.

Fig. 4*B* illustrates the changes in the measured individual rate constants for the ATPase cycle. Here, the changes were generally smaller than for the equilibrium constant, with no change compared with the WT values of >80% and mostly decreases. Overall, a pattern did not emerge of a common behavior of the DCM mutations.

The ATPase cycle

Values of the k_{cat} and K_m of the ATPase cycle for R403Q, R453C (HCM), and S532P (DCM) have been published (13, 14, 30), whereas those for I201T, A223T, R237W, and F764L are presented in Table 1 and Fig. S7. All k_{cat} values for the DCM constructs were lower than WT (between 30 and 70%). By comparison with HCM mutations, one HCM mutation increased the k_{cat} (R403Q) by ~30%, and the other (R453C) decreased by 17% (see Table 1 and Fig. 7). We modeled the complete cycle using all of our kinetic data and the ATPase values following the procedure we outlined in a recent paper comparing different myosin isoforms (16). Here, we modeled the ATPase cycle to provide estimates of the two missing parameters: the affinity of actin for the M·ADP·P_i complex $1/(K_5)$ and the rate of P_i release from A-M·ADP·P_i (k_{+6}). This allowed us to predict the occupancy of each myosin and actin·myosin states in the cycle as shown in Fig. 5. It is not clear what the effective actin concentration is in the rapidly shortening muscle (the nearest equivalent to the zero load conditions of the solution ATPase). In a rapidly shortening muscle, all active myosin heads have ready access to the actin as it moves past. Under isometric conditions, because of the mismatch of the thick and thin filament helicity, some myosin heads may have ready access to an actin site, whereas another cannot attach to actin at all. We therefore modeled a range of actin concentrations ([A] = K_m, 3 K_m, and 20 K_m, where the ATPase rate is 50, 87, and 98% of k_{cat} values, respectively) to facilitate comparison between the different mutant constructs under conditions that may match those of a contracting sarcomere. In addition, we attempted to model the situation when the muscle fiber is contracting under load. Here, we used the estimate for the inhibition of the ADP release rate constant under 5 pN of load as defined from loaded single-molecule assays: 3-fold inhibition (31, 32). We included a 3-fold reduction in both the ADP and P_i release rate constant to reproduce the expected ~3-fold reduction in ATPase cycling rate, which is not generated by a reduction in the ADP release rate constant alone.

The predicted occupancies are shown in Fig. 6. Note that the *color schemes* are the same in both Fig. 5 and Fig. 6; *red shades* indicate detached cross-bridges, *yellow shades* are weakly attached pre-force-holding cross-bridges, and *blue shades* represent strongly attached force-holding bridges. The *number* by each pie chart represents the percentage of the *pale blue*, force-holding A·M·D state. The previously published WT data predict at low actin concentration ([A] = K_m) almost 75% of cross-bridges are detached with just 6.8% in the force-holding *blue* states, dominated by the A·M·D state. As actin concentration is increased, the detached states (*red*) decrease, the weakly attached states (*yellow*) increase, and the strongly attached A·M·D state doubles to 13%. The application of a 5-pN load at [A] = 3 K_m increased the A·M·D state from 10.2 to 13.6% and increased the weakly attached states (mainly A-M·T) at the expense of the detached M·T state. A similar pattern was observed for all mutants studied. However, it is clear from an inspection of the images in Fig. 6 that all DCM constructs have a reduced occupancy of the force-holding, *blue-shaded* states and increases in the *yellow*, weakly attached bridges. The percentage of bridges in the force-holding A·M·D state is reduced in all cases, sometimes quite dramatically from 10.2% at [A] = 3 K_m for WT to <3% for S532P and R237W. In contrast, both HCM mutations have an increased occupancy of the A·M·D state (from 10.2 to 12.3 or 17.0% for R403Q and R453C, respectively, at [A] = 3 K_m). When bearing a load, all constructs increase the occupancy of the force-holding states (which is expected because load is modeled as a reduction of the rate at which ADP is released from A·M·D), but the extent of the

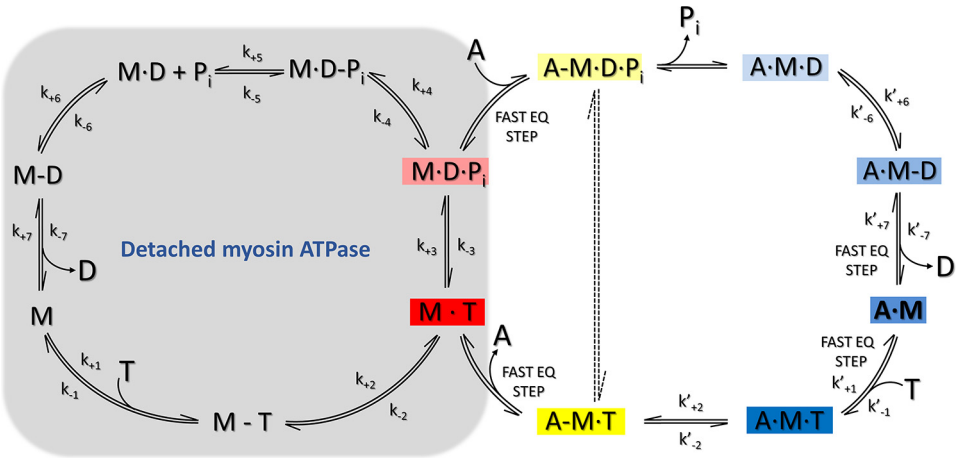

Figure 3. A minimal ATPase cycle for the myosin (seven-step) actin·myosin (nine-step) ATPase cycle. *M*, myosin; *A*, actin; *T*, ATP; *D*, ADP; *P*, P_i. In a complex, a *dot* means tight interaction between the components (*e.g.* A·M·D), and a *hyphen* indicates a relatively weak association (*e.g.* A·M-D). The rate constants for steps that we experimentally determined are given as k_{+j} in the forward (direction of ATP hydrolysis) and k_{-j} in the reverse direction, with K_i defined as k_{+}/k_i. The *background colors* of the given states correspond to the intermediates in the cross-bridge cycle in Fig. 5 and the *pie charts* in Fig. 6.

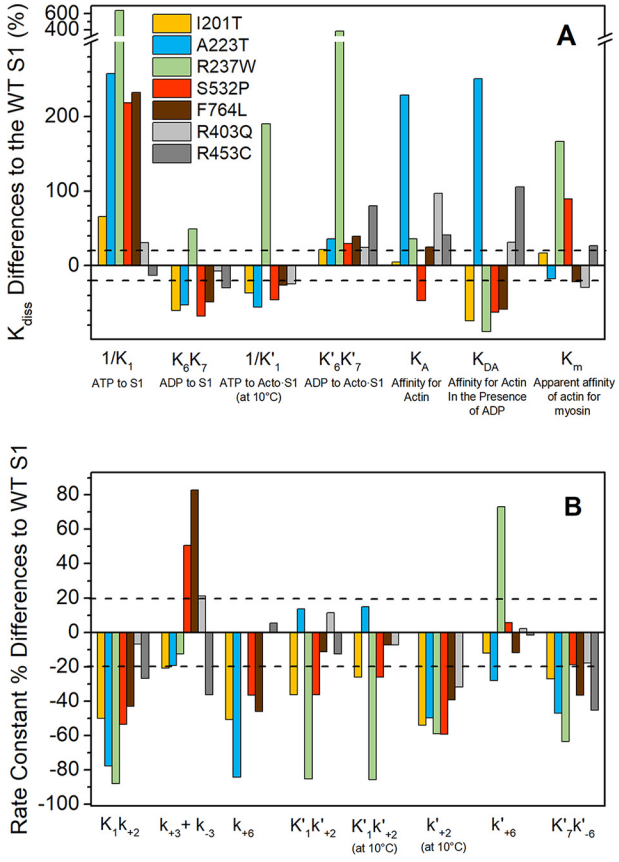

Figure 4. Summary of all of the percent change in each of the parameters measured in this study compared with WT. *A*, percent change compared with WT for the measured dissociation constant (K_A, K_{DA}), apparent K_m, or equilibrium constant for each of the steps as defined in Fig. 3. *B*, percent change in measured rate constants for each mutation compared with WT.

increase is very variable. For WT, a 5-pN load increases the A·M·D state from 10.8 to 13.6% (an approximately one-third increase). In contrast, the increases are predicted to be much smaller for the DCM mutations: 0.2% (less than one-tenth increase) for S532P and R237W and 0.8–1.5% for the other DCM mutations, whereas the R453C HCM mutant has a larger 5.5% (one-third) increase in the A·M·D state. The second HCM mutation, R403Q, has more A·M·D than WT with no load (12.3%) but increases by only a moderate 1.2% at 5-pN load, which is an increase of one-tenth (1.2%/12.3%).

These predictions for the lower occupancy of the A·M·D state during the ATPase cycle have the implication that in the steady state, the DCM constructs will bear less load, hence the need to activate more cross-bridges to hold the same force as the WT. This is seen from the modeling under load when a 5-pN load is applied to a single motor. In contrast, the HCM mutation can bear a larger load, as there will be more of the A·M·D in the steady state.

The effects on the key properties of the cross-bridge cycle are summarized in Fig. 7, where the measured k_{cat} values for the WT and each mutant are shown alongside the duty ratio, predicted V_{max}, the fractional occupancy of the A·M·D state, and how load is predicted to influence these parameters.

A clear pattern from these data is that the predicted duty ratios (dominated by the A·M·D state) are lower for four of five DCM mutants compared with WT, whereas for the HCM mutants, either no change or an increase is seen. This behavior is also seen under load, and although the duty ratio increases under load, the duty ratio remains lower than WT for the DCM constructs.

A single-molecule laser trap study of three of the DCM mutations used here (33) has recently been completed. This work estimated the duty ratio and the load dependence of the ADP release rate constant for each mutant. A maximum 10% change in the load dependence of the ADP step compared with WT was reported, and this was not statistically significant. The changes in duty ratio were similar to those estimated here.

The predicted velocity of shortening was estimated from the equation, $V_o = d{\cdot}ATPase/DR$ in each case, where d is the step size (assumed to be invariant), $ATPase$ is the measured ATPase, and DR is the predicted duty ratio. Note, as the ATPase and duty ratio have a similar strong dependence on actin concentration, the velocity is independent of actin concentration. As shown in Fig. 7 for k_{cat} of the ATPase and the predicted maximum velocity of shortening, there is no common pattern for DCM and HCM constructs.

Table 1

Measured parameters for the WT and 5 DCM linked mutations

Values for β WT myosin are from Nag *et al.* (14). Values differed significantly from WT, * $p < 0.05$, ** $p < 0.01$, *** $p < 0.001$. The color code indicates degree of difference from WT. *Blue*, slower rate constants or weaker equilibrium values; *red*, faster or stronger values. *Pale color* >30% <2-fold change; *dark shade*, ≥2-fold change compared to WT.

Parameter	WT	I201T	A223T	R237W	S532P	F764L
	N=3	N=3	N=3	N=3	N=3	N=3
ATP-binding to S1						
K_1k_{+2} (μM^{-1} s^{-1})	5.8 ± 0.2	2.9 ± 0.5**	1.3 ± 0.07***	0.7 ± 0.06***	2.7 ± 0.2***	3.3 ± 0.3**
$k_{+3} + k_{-3}$ (s^{-1})	91.2 ± 10.6	72.2 ± 4.4	73.6 ± 8.1	79.7 ± 4.0	137.3 ± 6.0*	166.8 ± 5.6**
$1/K_1$ (μM)	15.9 ± 2.2	26.4 ± 5.9	56.8 ± 6.5**	117.8 ± 7.0***	50.6 ± 1.1***	52.8 ± 5.0**
ADP-binding to S1						
K_6K_7 (μM)	0.53 ± 0.06	0.21 ± 0.03**	0.25± 0.01***	0.790 ± 0.124*	0.171 ± 0.01**	0.27 ± 0.04**
k_{+6} (s^{-1})	0.63 ± 0.03	0.31 ± 0.01***	0.1 ± 0.00***	Not measurable	0.4 ± 0.0**	0.34 ± 0.02***
ATP-binding to actin·S1						
$K'_1k'_{+2}$ (μM^{-1} s^{-1})	4.4 ± 0.3	2.8 ± 0.07*	5.0 ± 0.3	0.65 ± 0.07***	2.8 ± 0.03*	3.9 ± 0.4
$K'_1k'_{+2}$ (μM^{-1} s^{-1}) at 10 °C	2.7 ± 0.09	2.0 ± 0.2*	3.1 ± 0.1	0.39 ± 0.02***	2.0 ± 0.03**	2.5 ± 1
$1/K'_1$ (μM) at 10 °C	365.7 ± 17.7	230.7 ± 29.0*	161.3 ± 14.9***	1061.3 ± 67.1***	197.2 ± 3.0***	269.5 ± 30.3
k'_{+2} (s^{-1}) at 10 °C	991 ± 18.2	455.4 ± 22.0***	497.3 ± 27.8***	407.8 ± 14.0***	405.3 ± 4.2***	601.2 ± 23.8***
$K_{α1}$ at 10 °C	3.6 ± 0.3	2.6 ± 0.2	2.1 ± 0.03**	3.5 ± 0.4	2.2 ± 0.2*	3.5 ± 0.1
$k_{+α1}$ (s^{-1}) at 10 °C	78.9 ± 0.7	52.7 ± 5.5**	34.0 ± 0.5***	45.5 ± 3.4***	53.5 ± 2.6***	40 ± 2.7**
ADP-affinity for actin·S1						
$K'_6K'_7$ (μM)	6.1 ± 0.7	7.4 ± 0.6	8.3 ± 0.4	29.4 ± 2.6***	7.9 ± 0.3	8.5 ± 0.7
k'_{+6} (s^{-1})	58.7 ± 3.3	51.6 ± 2.3	42.3 ± 1.7*	101.6 ± 2.8***	62.0 ± 3.0	51.8 ± 2.8
$K'_7k'_{-6}$ (μM^{-1} s^{-1})	9.6	7.0	5.1	3.5	7.8	6.1
$K_{αD}$	No second phase	11.5 ± 3.2	No second phase	No second phase	7.1 ± 1.5	6.2 ± 1.8
$k_{+αD}$ (s^{-1})	No second phase	8.9 ± 1.7	No second phase	No second phase	8.4 ± 0.7	12.1 ± 3.6
$K'_6K'_7$ / K_6K_7	11.5	35.2	33.2	37.2	46.2	31.5
S1-affinity for actin						
K_A eq. (nM)	10 ± 1.8	10.5 ± 2.5	32.9 ± 3.0**	13.6 ± 0.8	5.3 ± 1.4	12.5 ± 0.9
K_{DA} (nM)	109.3 ± 13.8	28.3 ± 1.6**	382.9 ± 59.9*	12.8 ± 0.9**	41.0 ± 6.8**	45.3 ± 2.2**
K_{DA} / K_A	10.9	2.7	11.6	0.94	7.7	3.6
K_m (μM)‡	53.0 ± 5 (19)	46.33 ± 8 (6)	32.6 ± 6 (6)	105.5 ± 30 (4)*	74.9 ±	31 ± 10
k_{cat} (s^{-1}) ‡	5.5 ± 0.2 (19)	3.63 ± 0.3 (6)***	4.09 ± 0.3 (6)**	2.86 ± 0.5 (6)***	1.81 ± 0.1 (6)***	4.01 ±

‡ For the steady-state measurements, the data are the mean ± S.E. values from 4–6 independent measurements except the WT, which was the average from 19 samples. Experimental conditions were as follows: buffer 25 mM KCl, 5 mM $MgCl_2$ 20 mM MOPS, pH 7.0, 20 °C except the ATPase data, which used 10 mM imidazole, 5 mM KCl, 4 mM $MgCl_2$ and 23 °C.

Discussion

Overall, our data show only one difference that is common to four of the five DCM mutations, a reduced duty ratio (compared with WT) due to a lower occupancy of the force-holding A·M·D state, and this position is even clearer once the myosin cross-bridge is exposed to a 5-pN load. All other parameters assessed vary between the different mutations and thus reflect local influences of the mutation. The net result in each case is reduced force-holding capacity in the steady state.

What of the prediction that DCM and HCM mutations would be expected to show distinct behaviors? We have included our previously published kinetic data for two HCM mutations, R453C and R403Q, in Fig. 4 (*gray bars*). These again indicate no common pattern for the two HCM mutations nor a clear difference between the HCM and DCM data. The k_{cat} data for the ATPases are listed (see Table 1 and Fig. 7), and whereas one HCM mutation increased the k_{cat} by ~30% (R453C), the other (R403Q) decreased it by 17%. Note that all DCM mutations have a lower k_{cat} than the HCM mutations. The modeling of the ATPase cycle for R453C was included in our 2017 publication (16), and here, a similar analysis is reported for the R403Q mutation. The data are all included in Figs. 6–8 for comparison with the DCM data. Strikingly, Fig. 6 shows that in contrast to the DCM mutations, both HCM mutations have a higher duty ratio and an increase in occupancy of the A·M·D state (from 10.2 to 12.3 or 17.0% for R403Q and R453C, respectively, at [A] = 3 K_m), whereas the R453C HCM mutant has a larger 5.5% (one-third) increase in the A·M·D state. The second HCM mutation, R403Q, has more A·M·D than WT with no load (12.3%) but increases by only a modest 1.2% at 5-pN load. The modeling thus predicts that DCM mutations all predict a lower force-holding capacity in the steady state, whereas HCM mutations will have a higher force-holding capacity.

How do the mutations cause DCM?

This remains a difficult to answer question. The often repeated argument that HCM is a hypercontractile phenotype whereas DCM is hypocontractile derives from clinical echocardiographic data as well as contractility of some mouse models (34). The data have sometimes been used to predict hypo- and

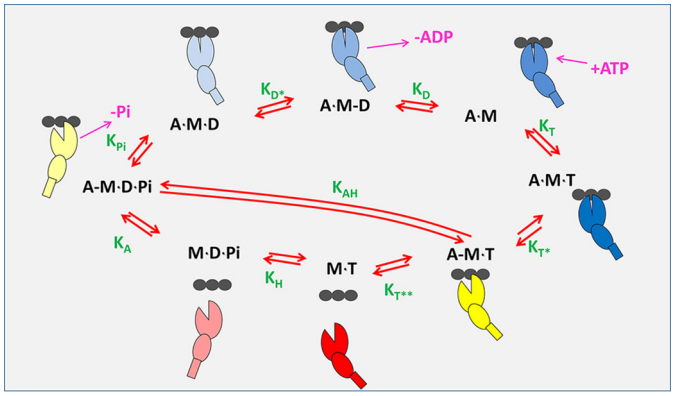

Figure 5. Actin·myosin ATPase–driven cross-bridge cycle. The *three black circles* represent three actin monomers. The other *symbol* represents the myosin motor domain. The *large ellipse* represents the majority of the myosin motor domain with the actin-binding site split by a cleft that is closed when tightly bound to actin. The *smaller ellipse* represents the converter domain, and the *rod* represents the lever arm/light chain–binding region. Strongly attached (to actin) force-holding states of the myosin are shown in *blue shades* (progressively *darker* going toward the rigor state). Weakly attached states (*yellow shades*) and detached states (*red shades*) are shown with the cleft open. Nucleotide and P_i binding and release steps are indicated in *cerise*, and *green lettering* indicates the equilibrium constants for each step of the cycle defined in the clockwise (ATP hydrolysis) direction. The steps are *labeled* with the equilibrium constant for each step in the forward direction as defined by Mijailovich *et al.* (16). The correspondence between these steps and those of Fig. 3 are shown in Table 1.

hyperactivity of individual myosin mutations, but this will depend upon which parameter is measured and in what isoform of myosin and what species. As shown in Fig. 7, a mutant myosin can be hypoactive in the k_{cat} of the ATPase activity and either hypoactive (A223T) or hyperactive (R237W) for velocity of shortening. The R453C HCM mutation has an increased duty ratio (better at holding force) yet lower velocity of shortening. Each parameter needs to be considered in terms of how it contributes to the overall performance. In addition, the data presented here are those expected for actin·myosin at full activation. The cardiac sarcomere is rarely fully activated, so how these results would be interpreted at submaximal activation also needs to be considered.

Activation and relaxation of contraction

Calcium regulation of the thin filament is perturbed by DCM or HCM mutations in the regulatory proteins troponin and tropomyosin and can result in loss or gain in calcium sensitivity (a decrease or increase in the calcium concentration required to half-activate contraction). For many mutations in thin filament proteins, a gain of calcium sensitivity is associated with HCM (35). The link between calcium sensitivity and DCM is not so clear cut; some *in vitro* work suggests a loss of sensitivity to β-adrenergic stimulation (36–39). Calcium sensitivity is also a function of the myosin ATPase cycle, as strongly bound cross-bridges can help activate the thin filament (40, 41). Thus, myosin mutations that increase the occupancy of the strongly bound states (and increase duty ratio), such as the two HCM mutations used, are expected to increase calcium sensitivity, and vice versa for the DCM mutations which decrease the duty ratio. This operates in the same way that reduction in ATP concentration or elevated ADP concentrations increase the duty ratio by slowing the detachment of rigor bridges, reducing calcium sensitivity.

The importance of activation of contraction via the thick filament has recently been highlighted (42, 43). Trivedi *et al.* (42) highlighted the potential of mutations in the myosin motor domain, myosin LC, S2, and MyBP-C, to alter the balance between relaxed and active states of the thick filament by altering the interaction between the myosin motors and the relaxed thick filament. The authors argue that this may be a common mechanism by which a large class of HCM mutations can produce hypercontractility (*i.e.* by increasing the number of myosin motors available for contraction). Many of the DCM residues studied here are buried and so are unlikely to affect motor domain–thick filament interaction directly. However, the other route by which myosin mutations can alter thick filament regulation is by altering the occupancy of the detached M·ADP·P_i state. This state (post-recovery-stroke, with switches 1 and 2 closed) is a prerequisite to form the stable so-called J-motif or interacting heads that form in the relaxed thick filament (44–46). Under relaxed conditions, the proportion of M·D·P_i is controlled by the equilibrium constant K_3 (Fig. 3). Any change here induced by a mutation could alter the balance between relaxed and active cross-bridges in the thick filament. During contraction, the proportion of myosin as M·ATP will be influenced by the equilibrium constant K_3 if the hydrolysis step can be treated as a rapid equilibrium step ($k_{+3} + k_{-3} \gg k_{cat}$) or by the value of $k_{+3} + k_{-3}$ if $k_{+3} + k_{-3}$ is of the same order as k_{cat}.

Energy balance

One suggestion for the causes of HCM and DCM phenotypes is that mutations induce a change in the energy balance of the cardiomyocytes by altering the efficiency with which the energy of ATP is utilized. This can be appreciated by estimating the energetic cost of force generation and movement. Here, the k_{cat} of the ATPase when generating 5 pN of force from Fig. 7 divided by 5 gives an energetic cost/pN force. This is shown in Fig. 8 (*top*) and estimates that individual WT β-cardiac myosin motors (or carrying either HCM mutation) use between 0.35 and 0.45 ATP s^{-1} per pN of load, whereas myosin carrying any of the DCM mutations uses 0.1–0.25 ATP s^{-1} for the same pN load.

In contrast, the energy used during unloaded shortening is given by $k_{cat} \times DR/d$. In other words, DR (the fraction of the ATPase cycle when movement is generated, which estimates the minimum number of myosins needed for smooth movement) divided by the step size d gives the ATP used per second for each nanometer of travel. As shown in Fig. 8 (*bottom*), this also suggests a distinction between HCM and DCM mutations. WT myosin used 0.16 ATP/s/nm of movement at V_{max} under zero load, whereas the two HCM constructs predict a higher ATP usage, 0.214 and 0.247 ATP/s/nm. In contrast, each DCM mutation is predicted to use much less ATP, and the velocities are slower (Fig. 5), but the ATP usage is also lower at between 0.014 and 0.106 ATP/s/nm (10–66% of WT values).

The estimates suggest that the DCM mutations generate less force and contract more slowly than WT myosin. The constructs also use ATP more economically at both high force and during high velocity contractions. The two HCM mutations are

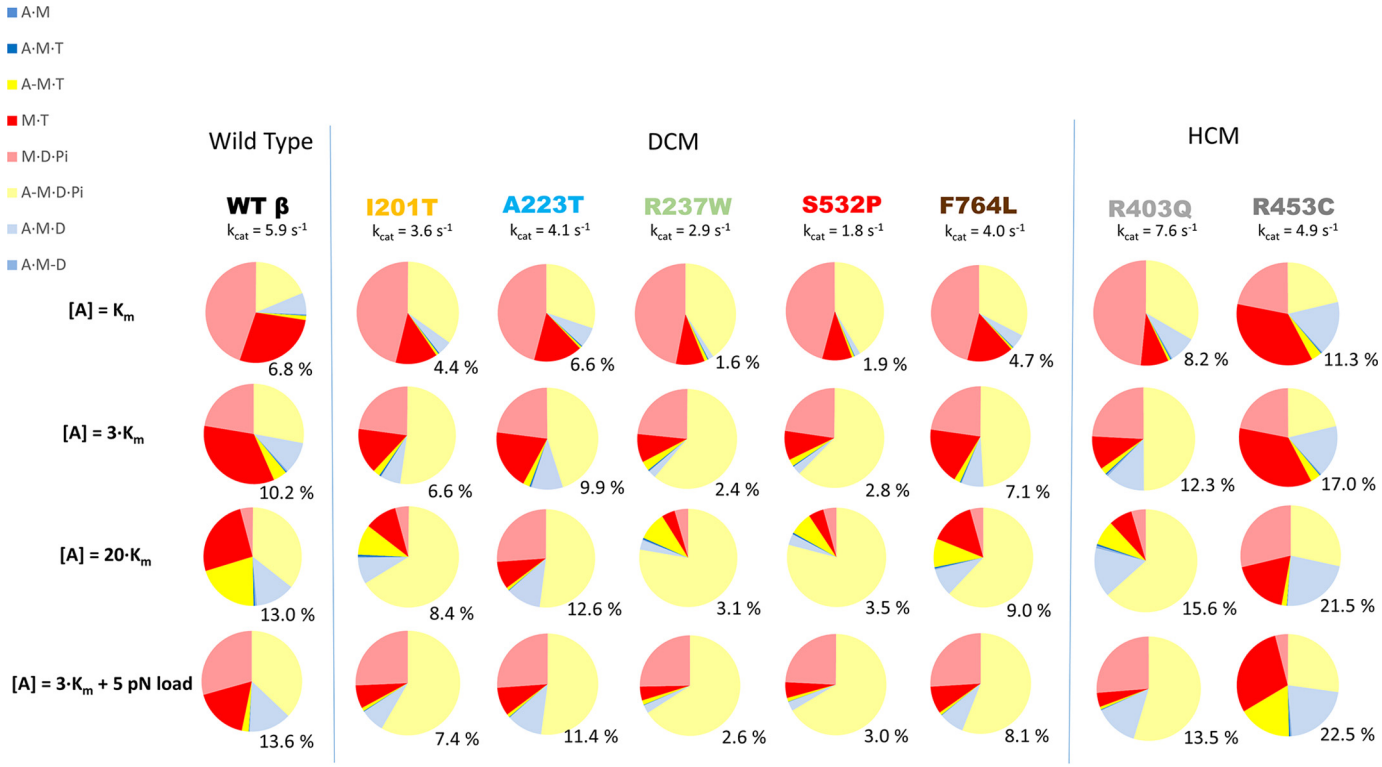

Figure 6. The occupancy of each of the intermediates in the ATPase cycle. The figure is *color-coded* to match the scheme in Fig. 5. The occupancy is shown at three actin concentrations, where [A] = K_m, 3 K_m, and 20 K_m. In addition, the result of what is predicted to happen to the state occupancies if the myosin bears a load of 5 pN at [A] = 3 K_m is shown.

more similar to WT in terms of the economy of force generation, whereas they are significantly less so for low load velocity.

An important caveat to the calculations presented here is that these are based on transient and steady-state biochemical kinetic assays. They assume that the step size *d* and the myosin stiffness remain unchanged by each of the mutations. A change in step size *d* will alter the distance moved in each ATPase cycle and will therefore alter the velocity of movement. A change in the step size or the stiffness of the motor domain will alter the force generated/held by each cross-bridge. A recent study (33) has shown that the load dependence of the ADP release step does not change significantly compared with WT for three of the DCM mutations studies here. Few studies of the step size for mutations in β-cardiac myosin have been made, but estimates of the step size for S532P are not distinguishable from WT (unpublished results).[7]

Comparison of predicted and measured in vitro velocities

In vitro motility measurements have been published for both of the HCM and one of the DCM mutations used here (13, 14, 30). Unpublished data[8] have been collected for the other DCM mutations with the exception of F764L. Each of these motility measurements used a construct with a C-terminal tag to allow specific attachment of the motor domain to the surface. Fig. 9 shows the mean velocity of the top 5% of smoothly moving filaments, normalized to the WT values, compared with our predictions (data in Fig. 7 and Table S5). A more complete analysis of the motility data is given in Table S1. The normalization to the WT values allows comparison between the two data sets despite the different constructs and different experimental conditions used. Caution must be taken with such comparisons, as a large number of measurements, each with its own error on the order of 20%, go into the calculation. When comparing experimental with predicted values, there is a correlation between the two values for four of six of the mutations (two DCMs and two HCMs), and the other 2 DCM mutations (S532P and R237W) show a predicted change that is ~35% greater than measured. For these two mutations, the calculation was affected by the very small estimates of the duty ratio, <0.05 in each case. A small error in this estimate can therefore have a large effect on the estimated velocity. In conclusion, where the estimate of the duty ratio is precise enough, there is a good correlation between the predicted and measured values, but the correlation breaks down when the duty ratio becomes too small to estimate with sufficient precision.

Testing our model predictions against experimental data will require more carefully matched experimental conditions and independent assessment of the step size for the same constructs. Note that our velocity calculations assume a constant step size for all of the mutations used here, which to date have not been measured.

Conclusions

The results presented here establish that the mutations alter individual steps in the ATPase cycle based on their specific location in the motor domain, but no common pattern has emerged for effects on specific steps associated with either

[7] J. Spudich and K. Ruppel, unpublished data.
[8] E. C. Yu, K. Ruppel, and J. Spudich, unpublished data.

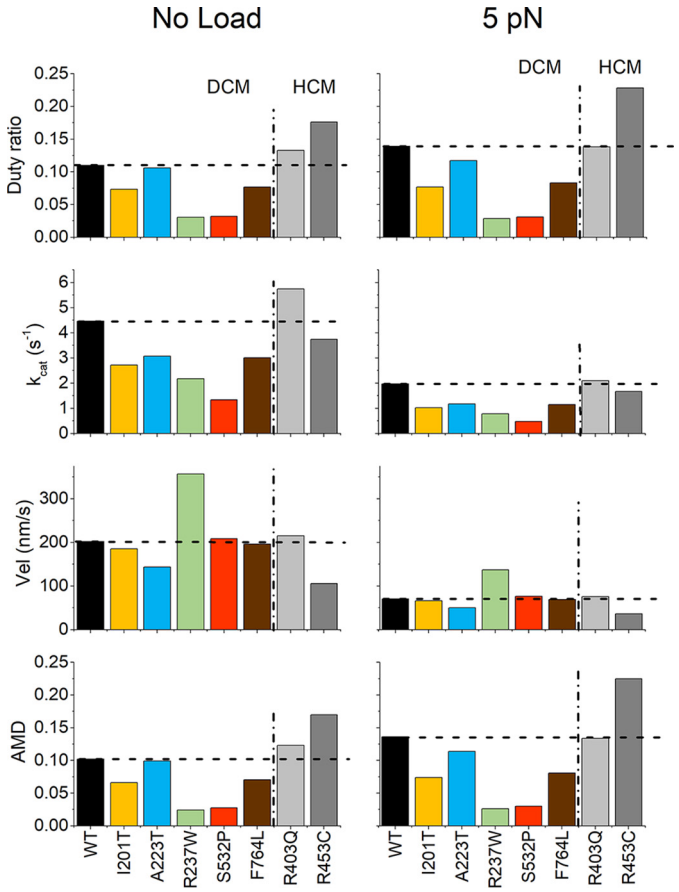

Figure 7. The calculated values for duty ratio, k_{cat}, shortening velocity, and occupancy of the force-holding A·M·D state for each of the mutations studied, plus those of previously published HCM mutations (R403Q and R453C). The *horizontal dotted line* indicates the value for the WT protein. The *vertical dash/dot line* separates the HCM and DCM mutations. The *left bar charts* (*red*) show the values based on the measured rate and equilibrium constants. The *right bar charts* are the predicted results if the myosin carries a 5-pN load.

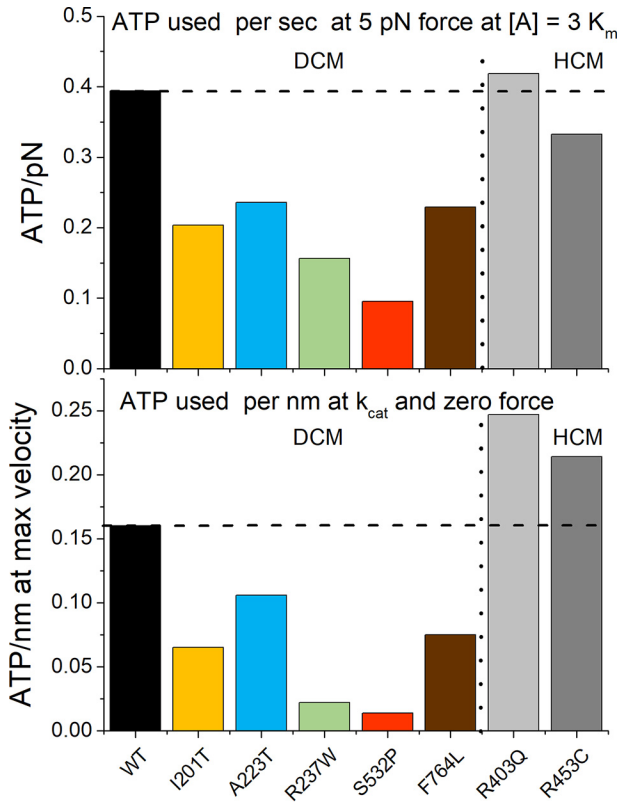

Figure 8. Economy of force generation and velocity for the DCM and HCM constructs. *Top*, ATP used per second per piconewton of force while generating 5 pN of force at [A] = 3 K_m. *Bottom*, ATP used per second at V_{max} of shortening (*i.e.* at k_{cat} for the ATPase ([A] = 20 K_m) and zero force (k_{cat} for the ATPase × *DR*/*d*)). Because ATPase and *DR* have the same dependence on [A], this calculation is the same at all concentrations of actin above K_m and only breaks down when the actin concentration becomes too low to maintain constant speed.

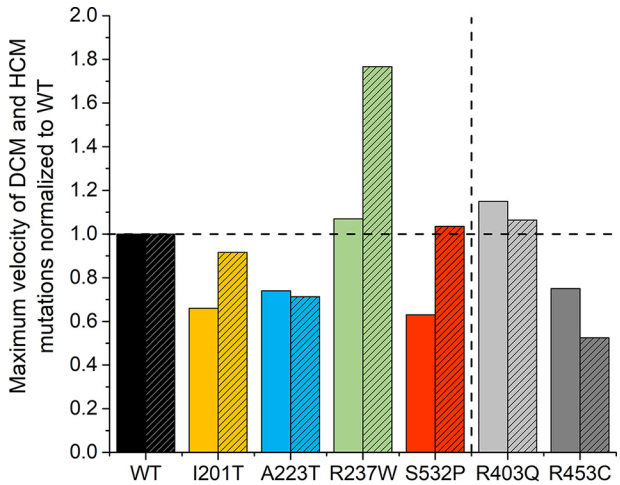

Figure 9. Comparison of normalized *in vitro* motility values to the predicted velocity of shortening. The *solid coloring* depicts the top 5% mean velocity values measured experimentally through unloaded *in vitro* motility and analyzed by the filament-tracking software described previously (30). The *bars* with *hatched patterns* are the values predicted from the kinetic analysis as described by Mijailovich (16) and given in Fig. 7 and Table S5. Similar to the modeling analysis, we are comparing the DCM mutations with the HCM mutations. Note that no data have been collected for the F764L mutant.

HCM or DCM mutations. However, when the cycle as a whole is considered, DCM and HCM mutations appear to alter the overall balance in the cycle in distinct ways. DCM mutations result in lower k_{cat} for the ATPase, a lower occupancy of the force-holding A·M·D state, and, hence, a lower duty ratio. The occupancy of the A·M·D state and the duty ratio are increased by a 5-pN load, but less than for the WT. Using these values to estimate the efficiency of ATP usage predicts that all DCM mutations here use less ATP to hold a 5-pN load than WT, whereas most also use less ATP to move 1 nm at V_{max}. Collectively, this study suggests that there is an overall loss of function concerning steady-state and motility parameters, leading to a deficit in force generation due to the reduced occupancy of the force-holding A·M·D state.

The same type of analysis of the two HCM mutations indicates a distinct behavior in several respects. The A·M·D state has higher occupancy than WT and hence a higher duty ratio. A 5-pN load for the R453C mutation increases the A·M·D state occupancy by one-third, much less for the R403Q mutation. The k_{cat} for the ATPase and the predicted velocity of shortening for the two HCM mutations change in opposite directions. In terms of ATP usage, the two HCM mutations both show a significant increase in the ATP used at high velocities compared with WT (the opposite of the DCM mutations), but a similar amount of ATP is needed per pN of force as in WT and more than the DCM mutations.

Thus, we have identified distinct differences between the HCM and DCM mutations in how they alter the mechanochemical cycle. DCM mutation show loss of contractile function across a range of properties, whereas HCM mutations have increased force-generating capacity but require greater ATP usage at high velocity compared with WT. How such changes result over a long period in the HCM or DCM phenotype remains to be explored.

The results presented here are for the behavior of a fully activated cross-bridge, yet cardiac sarcomeres are rarely fully activated. Additional factors will come into play at submaximal activation, where the altered behavior of the myosin heads will have secondary allosteric cooperative effects on both thick and thin filament activation. Importantly, the exact balance of properties of a specific mutation on contraction is likely to depend on the degree of penetrance in individual patients. This is an important consideration when extrapolating from studies with pure mutant proteins to the highly cooperative thick and thin filaments of the sarcomere.

Recently, there has been a resurgence of interest in the role of myosin thick filament regulation in defining the cooperativity of contractile activation and relaxation (for a review, see Refs. 42 and 43). The role of DCM and HCM mutations in such processes is only just beginning to be considered. Spudich (59) noted that many HCM mutations appear on a surface of the motor domain, which was termed the myosin mesa. The role of this myosin surface and its HCM mutations in the regulation of myosin activity via head–head interactions, in parking the heads onto the thick filament, and in interactions with MyBP-C has been explored (42, 47). Trivedi *et al.* (42) point out that such a mechanism can explain the hypercontractility phenotype of HCM by increasing the availability of myosin heads to contribute to contraction. In the final analysis, the effects of mutations on both the cross-bridge cycle and on the activation/relaxation processes will need to be considered.

Experimental procedures

Protein expression and purification

The production of adenovirus carrying the MYH7 motor domain and mutations therein as well as the infection and culturing of C_2C_{12} cells were performed as described (48). Recombinant human β-sS1 for both WT and DCM-causing mutations were co-expressed in C_2C_{12} cells with a His-tagged or a FLAG-tagged human ventricular ELC. For steady-state ATPase studies, the sS1 construct included a C-terminal enhanced GFP moiety (13), and the sS1 used for *in vitro* motility studies included a C-terminal 8-amino acid affinity clamp tag (30). The adenoviral particles were amplified using HEK293 cells; the viruses were purified using CsCl gradients, and the concentrated virus was stored in a glycerol buffer at −20 °C as described previously (27).

β-sS1 with a single ELC was purified by infecting C_2C_{12} cells for 4–5 days and frozen into cell pellets. Pellets were then homogenized in a low-salt buffer and centrifuged, and the supernatants were purified by affinity chromatography using either a HisTrap HP 1-ml column (His-ELC) or anti-FLAG resin (FLAG-ELC). In the case of His-tagged ELC–based purification, the sS1 was dialyzed into the low-salt stopped-flow buffer (25 mM KCl, 20 mM MOPS, 5 mM $MgCl_2$, 1 mM DTT, pH 7.0).

The sS1 elutes with a single light chain and what is assumed to be a small amount full-length endogenous myosin, which presumably binds the tagged light chain (Fig. 2). Dialysis in low-ionic strength stopped-flow buffer reduces the endogenous myosin to between 0.0 and 2.85% by molar ratio of motor domains. This is too low to have a significant effect on the transient measurements reported here. For FLAG-ELC–based purification, the sS1 was eluted from the anti-FLAG resin with excess FLAG peptide, and the eluate was run over an anion exchange column (HiTrap Q 1-ml column) as described (13).

Actin was prepared from rabbit muscle as described (49). The actin was labeled with pyrene at Cys-374 as described (50). For use at concentrations <1 μM, the actin was stabilized by incubation with phalloidin in a 1:1 mixture at 10 μM for several hours before use.

ATPase

Steady-state actin-activated ATPase activities for β-WT sS1 and the human cardiac mutant myosins were determined at 23 °C using a colorimetric assay to measure P_i production at various time points from a solution containing sS1, ATP, and increasing amounts of actin filaments (51). Assay buffer conditions were 10 mM imidazole, 5 mM KCl, 4 mM $MgCl_2$, and 1 mM DTT. Kinetic parameters (*i.e.* k_{cat}) were extracted from the data by fitting to the Michaelis–Menten equation using the curve-fitting toolbox in MATLAB (52).

Transient kinetics

All kinetic experiments were conducted in 20 mM MOPS buffer with 25 mM KCl, 5 mM $MgCl_2$, and 1 mM DTT, pH 7, at 20 °C, unless otherwise indicated. Measurements were performed with a High-Tech Scientific SF-61 DX2 stopped-flow system. The concentrations stated are those after mixing in the stopped-flow observation cell unless otherwise stated. All stopped-flow traces were analyzed in either software provided by TgK Scientific (Kinetic Studios) or Origin (Microcal). Intrinsic tryptophan fluorescence was measured by excitation at 295 nm and observed through a WG320 filter. In the absence of actin, the kinetics of S1 and ATP or ADP were interpreted using the seven-step model (53) (see Fig. 3), where the forward rate constants, in the counterclockwise direction, are k_{+i}, the reverse rate constants are denoted k_{-i}, and the equilibrium constant $K_i = k_{+i}/k_{-i}$. In the presence of actin, the data were interpreted in the equivalent scheme also shown in Fig. 3 (running clockwise), where the numbering of the reaction steps carries a prime (*e.g.* k'_{+1}, k'_{-1}, K'_1. The exception is the hydrolysis step (step 3), which is common to both cycles and is given as step 3 (no prime). The full details of each experimental measurement are given in Figs. S1–S6 in the supporting information.

Modeling

With the set of rate and equilibrium constants measured here and estimates of the k_{cat} and K_m values, it is possible to model the cycle in the steady state of ATP hydrolysis. Using the 8-state model of the actin·myosin ATPase cycle (shown in Fig. 5) and our measured constants, we were able to fit the model to the k_{cat} and K_m values to provide estimates for the actin affinity for

M·D·P (K_A) and the rate constant for P_i release (k_{+Pi}). Note that briefly, under standard steady-state conditions the P_i and ADP concentrations are assumed to be ~0. Thus, there is no rebinding of the products, P_i and ADP. This cycle can be modeled using any proprietary kinetic modeling program. We used the in-house MUSICO software as presented previously (16), as this allows fitting of the data to the steady-state parameters and provides error estimates of the fits, including the resolution matrix, which provided an estimate of the co-dependence of fitted parameters. As in our earlier modeling work on the WT β-cardiac and other myosin isoforms, all fitted parameters are well defined to a precision of ~20%. The resolution matrix values are consistent with parameters having low co-dependence (diagonal values close to 1), the exception being k_{-T}, which cannot be resolved from our current data. The fitted values of all constants and the resolution matrices are listed in Tables S1 and S2.

We modeled the effect of load on the cycle as set out in our 2017 paper (16). An estimate of the load dependence of ADP release comes from direct measurements of the effect of load on the lifetime of the AMD state (31, 32). We used 5 pN of load as an arbitrary value close to that thought to be likely for a muscle fiber under isometric tension, and the calculation suggests a 3-fold reduction in the ADP release rate constant. Such a reduction in the ADP release rate constant has little effect on the cycling rate of the system (ATPase). This is because the ADP release is 5–10-fold faster than k_{cat} and the reduction in the ADP rate constant is partially compensated by an increase in the occupancy of the AMD state. The combination of effects leaves the flux through the cycle little affected, yet there is a well-known inhibition of ATP turnover for a muscle fiber contracting against a load. For an isometric fiber, the ATPase has been estimated to be about one-third of the ATPase for a rapidly shortening muscle, a manifestation of the Fenn effect (54). The rate of entry into the force-holding or force-generating state is expected to be inhibited by load on thermodynamic arguments and is built into most models of the mechanical cross-bridge cycle (55, 56). We therefore applied a 3-fold inhibition of the ATPase cycling rate by reducing the entry into the force-holding state, k_{Pi} in our model. This assumes that the effect of load is similar on both P_i and ADP release steps. Such a model is not meant to be definitive but to illustrate the order of effect expected on the cycle.

Error analysis

In our previous paper (16), where we established this modeling approach, we demonstrated that varying any one of the fitted parameters (k_H, k_{-D}, K_{D^*}, k_{-D^*}, k_{-T^*}, K_{T^*}) by ±20% has minimal effect on the best fit values of the remaining parameters (*i.e.* the values varied by much less than 20%). This confirmed the findings of the sensitivity matrix that, apart from k_{-T}, the parameters are well defined by the fitting procedure. This observation remains true for the data presented here (see resolution matrices, Table S3). Here we additionally examined the influence of a change of 20% on the values of k_{cat} and K_m, used to define the fitted parameters.

K_m is largely controlled by the value of K_A. If K_m is altered by ±20%, then the value of $1/K_A$ ($1/K_A$ is used to have both in units of μM) changes by 20%. All other fitted parameters change by <5%. This is illustrated for the WT data in Table S7.

A 20% change in k_{cat} changes the flux through the system. For species like AMD, the rate constant k'_{+6} is fixed at the measured value. To change the flux through this step requires a 20% change in the concentration of AMD. Thus, AMD changes in line with the change in k_{cat}.

The effect of a change in k_{cat} on the fitted rate and equilibrium constants is variable, dependent upon how each rate constant contributes to the k_{cat} value, and this differs for each mutation. Because for most mutants, A-MDP_i is the predominant species in the steady state at high actin concentration, k_{Pi} will change to a similar extent as the change in k_{cat}. In other words, the flux through the P_i release step (essentially irreversible because $[P_i] = 0$) is equal to the ATPase rate; thus, $k_{cat} = k_{Pi} \times [\text{A-MDP}_i]/[M]_{total}$, and when actin is close to saturation, >60% of the myosin is in the A-MDP_i state (see Fig. 6 and Table S4), resulting in $k_{Pi} = 1.2–1.5 \times k_{cat}$.

Thus, varying k_{cat} by ±20% and refitting the data to generate new best-fit parameters has a significant effect on k_{Pi} (which changes by ~20%) but little effect on any other value. This is illustrated most clearly by the +20% data sets for S532P (no other fitted value changes by >3.2%) and F764L (no value changes by >8.3%; see data in Table S6), and a similar result is seen for A223T, R237W, and R403Q. A decrease in k_{cat} of 20% can be more significant, depending on the relationship to other steps in the cycle, namely k_H (see discussion below).

At the other end of the scale are WT and R453C, where k_{Pi} only partially limits the cycle. In the case of WT, A-MDP_i is ~35% of the total myosin at saturating actin, and the hydrolysis step is a significant contributor to the overall k_{cat} (*i.e.* k_H is similar to k_{Pi}). Changes of +20% in k_{cat} result in 30% change in k_{Pi} and 20% change in k_H. For R453C, 27% of the total myosin is as A-MDP_i and 29% as MT; thus, there is a significant shift toward the hydrolysis rate becoming limiting on the cycle, as reported (15). A change in k_{cat} now has a larger effect on both k_{Pi} (up to 50%) and k_H (16%), and this also results in a change in K_A.

Unloaded in vitro motility

Motility measurements were carried out as described (30, 57). Coverslips were coated with nitrocellulose and mounted on glass slides with double-sided tape for sample separation. sS1 with a C-terminal eight-amino acid affinity clamp was attached to the coverslip via a PDZ-18 anchor (30, 58). Actin filaments were monitored using a 1003 objective on a Nikon TiE microscope with at least four 30-s movies recorded for each condition. The mean velocity was calculated using the FAST software (30). We only report here the mean velocity for the top 5% of fastest filaments and then normalize those values to WT. All measurements were made at 23 °C.

Author contributions—M. A. G. and L. A. L. conceived the study and supervised each step of the work. Z. U. designed, performed, and analyzed the stopped-flow experiments with samples provided by C. D. V.; E. C. Y., K. M. R., and J. A. S. designed, performed, and analyzed the steady-state ATPases and *in vitro* motility experiments. Z. U., S. M. M., and M. S. completed the kinetic modeling. C. D. V. and Z. U. wrote the first draft of the paper. All authors contributed to the final version of the manuscript.

Acknowledgment—We thank Sam Lynn for assistance with actin preparations and general technical support.

References

1. Dellefave, L., and McNally, E. M. (2010) The genetics of dilated cardiomyopathy. *Curr. Opin. Cardiol.* **25,** 198–204 CrossRef Medline
2. Hershberger, R. E., Morales, A., and Siegfried, J. D. (2010) Clinical and genetic issues in dilated cardiomyopathy: a review for genetics professionals. *Genet. Med.* **12,** 655–667 CrossRef Medline
3. Richardson, P., McKenna, W., Bristow, M., Maisch, B., Mautner, B., O'Connell, J., Olsen, E., Thiene, G., Goodwin, J., Gyarfas, I., Martin, I., and Nordet, P. (1996) Report of the 1995 World Health Organization/International Society and Federation of Cardiology Task Force on the Definition and Classification of cardiomyopathies. *Circulation* **93,** 841–842 CrossRef Medline
4. Baig, M. K., Goldman, J. H., Caforio, A. L. P., Coonar, A. S., Keeling, P. J., and McKenna, W. J. (1998) Familial dilated cardiomyopathy: cardiac abnormalities are common in asymptomatic relative and may represent early disease. *J. Am. Coll. Cardiol.* **31,** 195–201 CrossRef Medline
5. Parvari, R., and Levitas, A. (2012) The mutations associated with dilated cardiomyopathy. *Biochem. Res. Int.* **2012,** 639250 Medline
6. McNally, E. M., and Mestroni, L. (2017) Dilated cardiomyopathy: genetic determinants and mechanisms. *Circ. Res.* **121,** 731–748 CrossRef Medline
7. Richard, P., Charron, P., Carrier, L., Ledeuil, C., Cheav, T., Pichereau, C., Benaiche, A., Isnard, R., Dubourg, O., Burban, M., Gueffet, J.-P., Millaire, A., Desnos, M., Schwartz, K., Hainque, B., *et al.* (2003) Hypertrophic cardiomyopathy: distribution of disease genes, spectrum of mutations, and implications for a molecular diagnosis strategy. *Circulation* **107,** 2227–2232 CrossRef Medline
8. Chang, A. N., and Potter, J. D. (2005) Sarcomeric protein mutations in dilated cardiomyopathy. *Heart Fail. Rev.* **10,** 225–235 CrossRef Medline
9. Kamisago, M., Sharma, S. D., DePalma, S. R., Solomon, S., Sharma, P., McDonough, B., Smoot, L., Mullen, M. P., Woolf, P. K., Wigle, E. D., Seidman, J. G., and Seidman, C. E. (2000) Mutations in sarcomere protein genes as a cause of dilated cardiomyopathy. *N. Engl. J. Med.* **343,** 1688–1696 CrossRef Medline
10. Daehmlow, S., Erdmann, J., Knueppel, T., Gille, C., Froemmel, C., Hummel, M., Hetzer, R., and Regitz-Zagrosek, V. (2002) Novel mutations in sarcomeric protein genes in dilated cardiomyopathy. *Biochem. Biophys. Res. Commun.* **298,** 116–120 CrossRef Medline
11. Hershberger, R. E., Parks, S. B., Kushner, J. D., Li, D., Ludwigsen, S., Jakobs, P., Nauman, D., Burgess, D., Partain, J., and Litt, M. (2008) Coding sequence mutations identified in *MYH7*, *TNNT2*, *SCN5A*, *CSRP3*, *LBD3*, and *TCAP* from 313 patients with familial or idiopathic dilated cardiomyopathy. *Clin. Transl. Sci.* **1,** 21–26 CrossRef Medline
12. Villard, E., Duboscq-Bidot, L., Charron, P., Benaiche, A., Conraads, V., Sylvius, N., and Komajda, M. (2005) Mutation screening in dilated cardiomyopathy: prominent role of the beta myosin heavy chain gene. *Eur. Heart J.* **26,** 794–803 CrossRef Medline
13. Sommese, R. F., Sung, J., Nag, S., Sutton, S., Deacon, J. C., Choe, E., Leinwand, L. A., Ruppel, K., and Spudich, J. A. (2013) Molecular consequences of the R453C hypertrophic cardiomyopathy mutation on human-cardiac myosin motor function. *Proc. Natl. Acad. Sci. U.S.A.* **110,** 12607–12612 CrossRef Medline
14. Nag, S., Sommese, R. F., Ujfalusi, Z., Combs, A., Langer, S., Sutton, S., Leinwand, L. A., Geeves, M. A., Ruppel, K. M., and Spudich, J. A. (2015) Contractility parameters of human β-cardiac myosin with the hypertrophic cardiomyopathy mutation R403Q show loss of motor function. *Sci. Adv.* **1,** e1500511 CrossRef Medline
15. Bloemink, M., Deacon, J., Langer, S., Vera, C., Combs, A., Leinwand, L., and Geeves, M. A. (2014) The hypertrophic cardiomyopathy myosin mutation R453C alters ATP binding and hydrolysis of human cardiac β-myosin. *J. Biol. Chem.* **289,** 5158–5167 CrossRef Medline
16. Mijailovich, S. M., Nedic, D., Svicevic, M., Stojanovic, B., Walklate, J., Ujfalusi, Z., and Geeves, M. A. (2017) Modeling the actin.myosin ATPase cross-bridge cycle for skeletal and cardiac muscle myosin isoforms. *Biophys. J.* **112,** 984–996 CrossRef Medline
17. Vikstrom, K. L., Factor, S. M., and Leinwand, L. A. (1996) Mice expressing mutant myosin heavy chains are a model for familial hypertrophic cardiomyopathy. *Mol. Med.* **2,** 556–567 Medline
18. Geisterfer-Lowrance, A. A. T., Christe, M., Conner, D. A., Ingwall, J. S., Schoen, F. J., Seidman, C. E., and Seidman, J. G. (1996) A mouse model of familial hypertrophic cardiomyopathy. *Science* **272,** 731–734 CrossRef Medline
19. McConnell, B. K., Fatkin, D., Semsarian, C., Jones, K. A., Georgakopoulos, D., Maguire, C. T., Healey, M. J., Mudd, J. O., Moskowitz, I. P., Conner, D. A., Giewat, M., Wakimoto, H., Berul, C. I., Schoen, F. J., Kass, D. A., *et al.* (2001) Comparison of two murine models of familial hypertrophic cardiomyopathy. *Circ. Res.* **88,** 383–389 CrossRef Medline
20. Schmitt, J. P., Debold, E. P., Ahmad, F., Armstrong, A., Frederico, A., Conner, D. A., Mende, U., Lohse, M. J., Warshaw, D., Seidman, C. E., and Seidman, J. G. (2006) Cardiac myosin missense mutations cause dilated cardiomyopathy in mouse models and depress molecular motor function. *Proc. Natl. Acad. Sci. U.S.A.* **103,** 14525–14530 CrossRef Medline
21. Debold, E. P., Schmitt, J. P., Patlak, J. B., Beck, S. E., Moore, J. R., Seidman, J. G., Seidman, C., and Warshaw, D. M. (2007) Hypertrophic and dilated cardiomyopathy mutations differentially affect the molecular force generation of mouse α-cardiac myosin in the laser trap assay. *Am. J. Physiol. Heart Circ. Physiol.* **293,** H284–H291 CrossRef Medline
22. Lowey, S., Lesko, L. M., Rovner, A. S., Hodges, A. R., White, S. L., Low, R. B., Rincon, M., Gulick, J., and Robbins, J. (2008) Functional effects of the hypertrophic cardiomyopathy R403Q mutation are different in an α- or β-myosin heavy chain backbone. *J. Biol. Chem.* **283,** 20579–20589 CrossRef Medline
23. Geeves, M. A., and Holmes, K. C. (2005) The molecular mechanism of muscle contraction. *Adv. Protein Chem.* **71,** 161–193 CrossRef Medline
24. Geeves, M. A., Fedorov, R., and Manstein, D. J. (2005) Molecular mechanism of actomyosin-based motility. *Cell. Mol. Life Sci.* **62,** 1462–1477 CrossRef Medline
25. Sweeney, H. L., and Houdusse, A. (2010) Structural and functional insights into the myosin motor mechanism. *Annu. Rev. Biophys.* **39,** 539–557 CrossRef Medline
26. Adamek, N., Geeves, M. A., and Coluccio, L. M. (2011) Myo1c mutations associated with hearing loss cause defects in the interaction with nucleotide and actin. *Cell. Mol. Life Sci.* **68,** 139–150 CrossRef Medline
27. Deacon, J. C., Bloemink, M. J., Rezavandi, H., Geeves, M. A., and Leinwand, L. A. (2012) Identification of functional differences between recombinant human α and β cardiac myosin motors. *Cell. Mol. Life Sci.* **69,** 2261–2277 CrossRef Medline
28. Bloemink, M. J., Deacon, J. C., Resnicow, D. I., Leinwand, L. A., and Geeves, M. A. (2013) The superfast human extraocular myosin is kinetically distinct from the fast skeletal IIa, IIb, and IId isoforms. *J. Biol. Chem.* **288,** 27469–27479 CrossRef Medline
29. Bloemink, M. J., Adamek, N., Reggiani, C., and Geeves, M. A. (2007) Kinetic analysis of the slow skeletal myosin MHC-1 isoform from bovine masseter muscle. *J. Mol. Biol.* **373,** 1184–1197 CrossRef Medline
30. Aksel, T., Choe Yu, E., Sutton, S., Ruppel, K. M., and Spudich, J. A. (2015) Ensemble force changes that result from human cardiac myosin mutations and a small-molecule effector. *Cell Rep.* **11,** 910–920 CrossRef Medline
31. Greenberg, M. J., Shuman, H., and Ostap, E. M. (2014) Inherent force-dependent properties of β-cardiac myosin contribute to the force-velocity relationship of cardiac muscle. *Biophys. J.* **107,** L41–L44 CrossRef Medline
32. Sung, J., Nag, S., Mortensen, K. I., Vestergaard, C. L., Sutton, S., Ruppel, K., Flyvbjerg, H., and Spudich, J. A. (2015) Harmonic force spectroscopy measures load-dependent kinetics of individual human β-cardiac myosin molecules. *Nat. Commun.* **6,** 7931 CrossRef Medline
33. Liu, C., Kawana, M., Song, D., Ruppel, K. M., and Spudich, J. A. (2018) Controlling load-dependent contractility of the heart at the single molecule level. *bioRxiv* 258020 CrossRef
34. Seidman, J. G., and Seidman, C. (2001) The genetic basis for cardiomyopathy. *Cell* **104,** 557–567 CrossRef Medline

35. Westfall, M. V., Borton, A. R., Albayya, F. P., and Metzger, J. M. (2002) Myofilament calcium sensitivity and cardiac disease: insights from troponin I isoforms and mutants. *Circ. Res.* **91,** 525–531 CrossRef Medline
36. Molkentin, D. J., and Dorn, G. W., 2nd (2001) Cytoplasmic signaling pathways that regulate cardiac hypertrophy. *Annu. Rev. Physiol.* **63,** 391–426 CrossRef Medline
37. Minamisawa, S., Hoshijima, M., Chu, G., Ward, C. A., Frank, K., Gu, Y., Martone, M. E., Wang, Y., Ross, J., Jr., Kranias, E. G., Giles, W. R., and Chien, K. R. (1999) Chronic phospholamban-sarcoplasmic reticulum calcium atpase interaction is the critical calcium cycling defect in dilated cardiomyopathy. *Cell* **99,** 313–322 CrossRef Medline
38. Messer, A. E., and Marston, S. B. (2014) Investigating the role of uncoupling of troponin I phosphorylation from changes in myofibrillar Ca^{2+}-sensitivity in the pathogenesis of cardiomyopathy. *Front. Physiol.* **5**, 315 CrossRef Medline
39. Memo, M., Leung, M. C., Ward, D. G., dos Remedios, C., Morimoto, S., Zhang, L., Ravenscroft, G., McNamara, E., Nowak, K. J., Marston, S. B., and Messer, A. E. (2013) Familial dilated cardiomyopathy mutations uncouple troponin i phosphorylation from changes in myofibrillar Ca^{2+} sensitivity. *Cardiovasc. Res.* **99,** 65–73 CrossRef Medline
40. Geeves, M. A. (2012) Thin filament regulation. In *Comprehensive Biophysics*, Vol. 4, pp. 251–267, Elsevier B.V., Amsterdam
41. Gordon, A. M., Homsher, E., and Regnier, M. (2000) Regulation of contraction in striated muscle. *Physiol. Rev.* **80,** 853–924 CrossRef Medline
42. Trivedi, D. V., Adhikari, A. S., Sarkar, S. S., Ruppel, K. M., and Spudich, J. A. (2017) Hypertrophic cardiomyopathy and the myosin mesa: viewing an old disease in a new light. *Biophys. Rev.* 10.1007/s12551-017-0274-6
43. Irving, M. (2017) Regulation of contraction by the thick filaments in skeletal muscle. *Biophys. J.* **113,** 2579–2594 CrossRef Medline
44. Wendt, T., Taylor, D., Trybus, K. M., and Taylor, K. (2001) Three-dimensional image reconstruction of dephosphorylated smooth muscle heavy meromyosin reveals asymmetry in the interaction between myosin heads and placement of subfragment 2. *Proc. Natl. Acad. Sci. U.S.A.* **98,** 4361–4366 CrossRef Medline
45. Nyitrai, M., Stafford, W. F., Szent-Györgyi, A. G., and Geeves, M. A. (2003) Ionic interactions play a role in the regulatory mechanism of scallop heavy meromyosin. *Biophys. J.* **85,** 1053–1062 CrossRef Medline
46. Kalabokis, V. N., and Szent-Györgyi, A. G. (1997) Cooperativity and regulation of scallop myosin and myosin fragments. *Biochemistry* **36,** 15834–15840 CrossRef Medline
47. Nag, S., Trivedi, D. V., Sarkar, S. S., Adhikari, A. S., Sunitha, M. S., Sutton, S., Ruppel, K. M., and Spudich, J. A. (2017) The myosin mesa and the basis of hypercontractility caused by hypertrophic cardiomyopathy mutations. *Nat. Struct. Mol. Biol.* **24,** 525–533 CrossRef Medline
48. Walklate, J., Vera, C., Bloemink, M. J., Geeves, M. A., and Leinwand, L. (2016) The most prevalent freeman-sheldon syndrome mutations in the embryonic myosin motor share functional defects. *J. Biol. Chem.* **291,** 10318–10331 CrossRef Medline
49. Spudich, J. A., and Watt, S. (1971) The regulation of rabbit skeletal muscle contraction. *J. Biol. Chem.* **246,** 4866–4871
50. Criddle, A. H., Geeves, M. A., and Jeffries, T. (1985) The use of actin labelled with *N*-(1-pyrenyl) iodoacetamide to study the interaction of actin with myosin subfragments and troponin/tropomyosin. *Biochem. J.* **232,** 343–349 CrossRef Medline
51. Trybus, K. M. (2000) Biochemical studies of myosin. *Methods* **22,** 327–335 CrossRef Medline
52. De La Cruz, E. M., and Ostap, E. M. (2009) *Kinetic and Equilibrium Analysis of the Myosin ATPase*, 1st Ed., Elsevier Inc., Amsterdam
53. Bagshaw, C. R., and Trentham, D. R. (1974) The characterization of myosin–product complexes and of product-release steps during the magnesium ion-dependent adenosine triphosphatase reaction. *Biochem. J.* **141,** 331–349 CrossRef Medline
54. Fenn, W. O. (1923) A quantitative comparison between the energy liberated and the work performed by the isolated sartorius muscle of the frog. *J. Physiol.* **58,** 175–203 CrossRef Medline
55. Smith, D. A. (2014) A new mechanokinetic model for muscle contraction, where force and movement are triggered by phosphate release. *J. Muscle Res. Cell Motil.* **35,** 295–306 CrossRef Medline
56. Smith, D. A., and Geeves, M. A. (1995) Strain-dependent cross-bridge cycle for muscle. II. Steady-state behavior. *Biophys. J.* **69,** 538–552 CrossRef Medline
57. Adhikari, A. S., Kooiker, K. B., Sarkar, S. S., Liu, C., Bernstein, D., Spudich, J. A., and Ruppel, K. M. (2016) Early-onset hypertrophic cardiomyopathy mutations significantly increase the velocity, force, and actin-activated ATPase activity of human β-cardiac myosin. *Cell Rep.* **17,** 2857–2864 CrossRef Medline
58. Huang, J., Nagy, S. S., Koide, A., Rock, R. S., and Koide, S. (2009) A peptide tag system for facile purification and single-molecule immobilization. *Biochemistry* **48,** 11834–11836 CrossRef Medline
59. Spudich, J. A. (2015) The myosin mesa and a possible unifying hypothesis for the molecular basis of human hypertrophic cardiomyopathy. *Biochem. Soc. Trans.* **43,** 64–72 CrossRef Medline

Dilated cardiomyopathy myosin mutants have reduced force-generating capacity

Zoltan Ujfalusi, Carlos D. Vera, Srbolujub M. Mijailovich, Marina Svicevic, Elizabeth Choe Yu, Masataka Kawana, Kathleen M. Ruppel, James A. Spudich, Michael A. Geeves and Leslie A. Leinwand

J. Biol. Chem. 2018, 293:9017-9029.
doi: 10.1074/jbc.RA118.001938 originally published online April 17, 2018